

Developing a Finite Element Model for Thermal Analysis of Friction Stir Welding (FSW) Using Hyperworks



Bahman Meyghani and Mokhtar Awang

Abstract The study undertakes a three-dimensional finite element analysis of the friction stir welding (FSW) process of 6061-T6 aluminium alloy. The analysis investigates the temperature distribution and the fundamental knowledge of the process with respect to temperature difference in the material to be welded. HyperMesh® and HyperView® solver have been used from Altair Hyperworks® to analyse the process. Different traverse and rotational speeds have been applied in the model. The results of the study create a better understanding for peak temperature distribution. In addition, the results illustrate that the peak temperature during welding increases as the rotational speeds rises and the effect of the transverse speed on the temperature is found to be insignificant. Finally, comparisons with some published papers has been done in order to compare the results of the different finite element packages and summarize the advantages and disadvantages of each software.

Keywords Friction Stir Welding · Thermal analysis · Temperature distribution · Heat Affected Zone · Hyperworks

1 Introduction

Friction Stir Welding (FSW) contains some stages including plunging, welding and retracting (plunging out). It needs to be mentioned that there are two significant causes for the heat generation in this process: friction force and plastic deformation ‘cold work’ [1–5]. There is a rotating, cylindrical, and non-consumable tool in FSW which has a pin and a shoulder (that can have different shapes). During the plunging of the tool inside the workpiece, the contact between the tool and the workpiece

B. Meyghani

Institute of Materials Joining, Shandong University, Jinan 250061, People’s Republic of China

M. Awang (✉)

Department of Mechanical Engineering, Faculty of Engineering, Universiti Teknologi

PETRONAS, 32610 Bandar Seri Iskandar, Perak Darul Ridzuan, Malaysia

e-mail: mokhtar_awang@utp.edu.my

© Springer Nature Singapore Pte Ltd. 2020

M. Awang et al. (eds.), *Advances in Material Sciences and Engineering*, Lecture Notes in Mechanical Engineering, https://doi.org/10.1007/978-981-13-8297-0_64

619

generates heat. In some cases, there is a dwelling step in order to assist in softening of the material, then the tool is ready to move across the welding seam and join the plates.

It should be mentioned that the ability of the tool for producing a good processed zone depends on the life of the tool [6]. One of the key parameters that affects the tool life is the heat generated during FSW. The range of temperature has been specified to ensure good material flow and good stirring of the materials [7]. Fehrenbacher et al. [7] reported that at the shoulder temperature of 515 °C, defects were come across in the welds for AA6061. Nevertheless, welding at above solidus temperature has led to the degradation in the weld quality, thus, indicating that local melting had occurred. In the contrary, at shoulder temperature of 533 °C, the welds performed a higher quality weld [7]. A decrement of the ultimate tensile strength of the welds were also reported once the solidus temperature was achieved during welding. Additionally, grain growth can also be enhanced during higher welding temperatures [7].

It needs to be mentioned that finite element methods are appropriate for investigating of the temperature behaviour during the process more in detail, save time and the manufacturing costs. Different finite element models have been used so far for modelling the process [8–12] including Eulerian [4], Lagrangian and Arbitrary Eulerian Lagrangian [9, 13] for welding of different materials [5, 14, 15]. Although, all of the above-mentioned studies have used refine mesh technique, however the distortion of mesh is still one of the most significant problems for modelling the FSW. To illustrate the issue, the deformation of the material during the process is large and this issue causes the distortion of mesh. The capability of the quick generation of high-quality mesh is one of the core competencies of HyperMesh[®], therefore by using this software the mesh distortion problem can be solved. Moreover, the direct recording of the temperature in the nugget zone is difficult, however by employing finite element modelling the behaviour of the temperature inside the nugget zone can be investigated. Thus, the purpose of this study is to explore the peak temperature in the vicinity of the tool-workpiece by using high-performance finite element modelling commercial software Altair Hyperworks[®]. Finally, the findings have been validated and the model is confirmed by comparing the results with published papers.

2 Methodology

2.1 Finite Element Model Descriptions

Aluminium 6061-T6 alloy is used for the plates and the tool material is steel H13. The dimension of the plate is 200 mm in length, 100 mm in width and 10 mm in thickness. The shoulder diameter is 18 mm and length of the pin is 6 mm. Figure 1a shows the tool description and Fig. 1b indicates the assembled model. It needs to be mentioned that the shoulder penetration depth inside the workpiece is set to be



Fig. 1 **a** The tool, **b** the assembled model including the tool and the workpiece

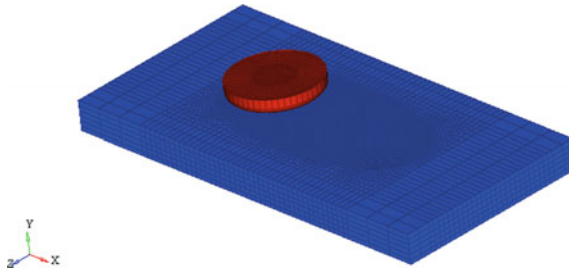


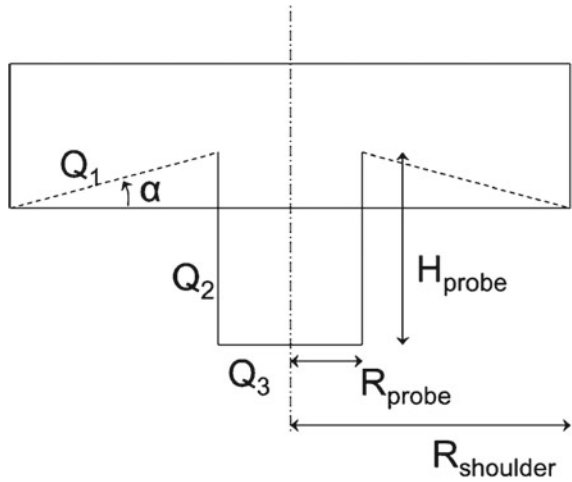
Fig. 2 The explanation of the mesh for the workpiece and the tool

0.15 mm. Furthermore, different rotational (800, 1200 and 1600 RPM) and transverse velocities (40, 70 and 100 mm/min) have been applied to the model.

Three dimensional (3D) finite element thermo-mechanical analysis type is used for the simulation. The finite element assumptions are applied in the model such as temperature dependent values of the friction coefficient which is calculated by Meyghani et al. [3, 16, 17]. In addition, different temperature dependent material properties have been applied in the model [18] including thermal conductivity, specific heat and density. As can be observed in Fig. 2, CTD8RT element is selected for the welding, total number of nodes are 28,357 and the total number of elements are 23,832.

RADIOSS™ solver is established around 30 years ago. It has been used in different problems such as the crash of the automotive, drop and impact analysis, terminal ballistic, blast and explosion effects and high velocity impacts. It should be noted that, in all of the abovementioned problems, large plastic deformation is present. Moreover, in complex environments such as aerospace, defence companies, automotive, electronics, and R&D centres for understanding and predicting the behaviour of the design, HyperWorks® environment is used and this issue makes RADIOSS™ as an appropriate tool for designing and analysing the problem. Therefore, in this research Altair RADIOSS™ solver is employed in order to solve the problem, because this solver is a leading structural analysis solver and can be employed for highly non-linear problems under dynamic loadings.

Fig. 3 FSW tool with a conical shoulder and a cylindrical unthreaded pin



2.2 Heat Generation Theoretical Background

Figure 3 shows the total heat generation at different areas of the tool [19] which are sub-divided into different components of the tool interface, including the generated heat at the shoulder bottom Q_1 , at the pin side Q_2 and at the tool pin bottom Q_3 .

The general expression for the heat generation is defined as,

$$Q = \omega T_{total} \tag{1}$$

where ω is the rotating velocity and T_{total} is the magnitude of the total torque which depends on different quantities: the force applied to the welding tool, the length of the lever arm linking the axis to the point of force application, and the angle between the lever arm and the force vector. The value of the torque is equal to,

$$T_{total} = \vec{r} \cdot \vec{F} \tag{2}$$

where r is the position vector and F is the force vector, therefore,

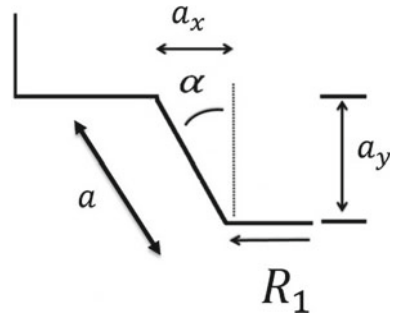
$$Q = \omega \vec{r} \cdot \vec{F} \tag{3}$$

According to the shear stress formula, the force vector is equal to,

$$\vec{F} = \vec{\tau} \cdot A \tag{4}$$

where τ is the shear stress and A is the area of the tool that are involved in producing the friction force, including A_S which is the region of the shoulder bottom, A_{pb} which is the pin bottom area and A_{ps} which is the pin side region, therefore,

Fig. 4 Schematic view of the tool and the pin side area



$$Q = \omega \vec{r} \cdot \vec{\tau} A \tag{5}$$

The formula for calculating average heat generation per unit area can be written as follows,

$$dQ = \omega \vec{r} \cdot \vec{\tau} dA \tag{6}$$

where dA can be written as,

$$dA = \vec{r} dr d\theta \tag{7}$$

Therefore, an integral can be summarized for calculating the generated heat in all areas, for example, for the shoulder bottom area (Q_1), the value of the generated heat can be explained as follows,

$$Q_1 = \oint_{A_S} \omega \tau_0 dA_S = \int_0^{2\pi} \int_{R_1}^{R_S} \omega \tau_0 \cdot r^2 dr d\theta = \omega \tau_0 \frac{2}{3} \pi (R_S^3 - R_1^3) \tag{8}$$

For finding the heat generation at the pin side area, firstly the region of the pin side (A_{PS}) which is explained in Fig. 4 needs to be investigated.

where $a = \sqrt{a_x^2 + a_y^2}$, in which $a_x = R_2$ and $a_y = H$, where H is the pin height, therefore, $(R_2 + H \tan \alpha) = A_{PS}$. For the pin side area, the generated heat (Q_2) is equal to,

$$\begin{aligned} Q_2 &= \oint_{A_{PS}} \omega \tau_1 dA_{PS} = \int_0^{2\pi} \int_0^H \omega \tau_1 (R_2 + H \tan \alpha)^2 dH d\theta \\ &= \omega \tau_1 \frac{2}{3} \pi (R_2^2 H + 3R_2 H^2 \tan \alpha + H^3 \tan^2 \alpha) \end{aligned} \tag{9}$$

The generated heat for the pin bottom area (Q_3) can be calculated as,

$$Q_3 = \oint_{A_{pb}} \omega \tau_0 dA_{pb} = \int_0^{2\pi} \int_0^{R_2} \omega \tau_0 r^2 dr d\theta = \omega \tau_0 \frac{2}{3} \pi (R_2^3) \quad (10)$$

Finally, the total generated heat is denoted by gathering all generated heats in different areas, the shoulder bottom Q_1 , the pin side Q_2 and the pin bottom Q_3 as follows,

$$Q_{total} = \oint_{A_S} \omega \tau_0 dA_S + \oint_{A_{pb}} \omega \tau_0 dA_{pb} + \oint_{A_{ps}} \omega \tau_1 dA_{ps}$$

$$Q_{total} = Q_1 + Q_2 + Q_3 \quad (11)$$

Therefore, the summarize of the above-mentioned values will be the overall amount of the produced heat during the process. It can be concluded that the geometry of the contact area, rotational velocity, the force and the shear stress will affect the generation of the heat during FSW.

3 Results and Discussion

A couple thermo mechanical finite element model is considered for the simulation. As can be observed in Fig. 5 the welding temperature is increased as the tool penetrates inside the plates. It is obtained that the temperature of the welding at the tool trailing edge is more than the other parts. Moreover, the temperature of the welding advancing side is always more than the temperature of the welding retreating side. This issue happens due to the difference in the conduction of the heat at different welding sides. To illustrate the issue, the solid material starts to move from the welding advancing side to the welding retreating side, therefore the movement of heat from the solid material which is located in the advancing side to another side causes difference temperature values. Furthermore, the results indicate that the slipping rate of the front side and the retreating side are lower than the back side and the advancing side.

It is also detected that the heat produces by the shoulder is more than the heat that is generated by the pin (Fig. 6), therefore the upper surface temperature is always higher than the bottom surface temperature (around 60 °C higher). In addition, it is observed that as the distance from the welding centre line increases the difference between the temperature of the upper and the lower surface is decreased.

The highest heat is generated inside the nugget zone (NZ) and the maximum heat dissipation is obtained from the NZ (happened close to the shoulder edge contact area). The contours of the gradient of the temperature at the upper surface in the horizontal-side (longitudinal side) is shown in Fig. 6, which verifies that the area contacted with the shoulder lateral surface is exposed to the higher temperature gradient effect.

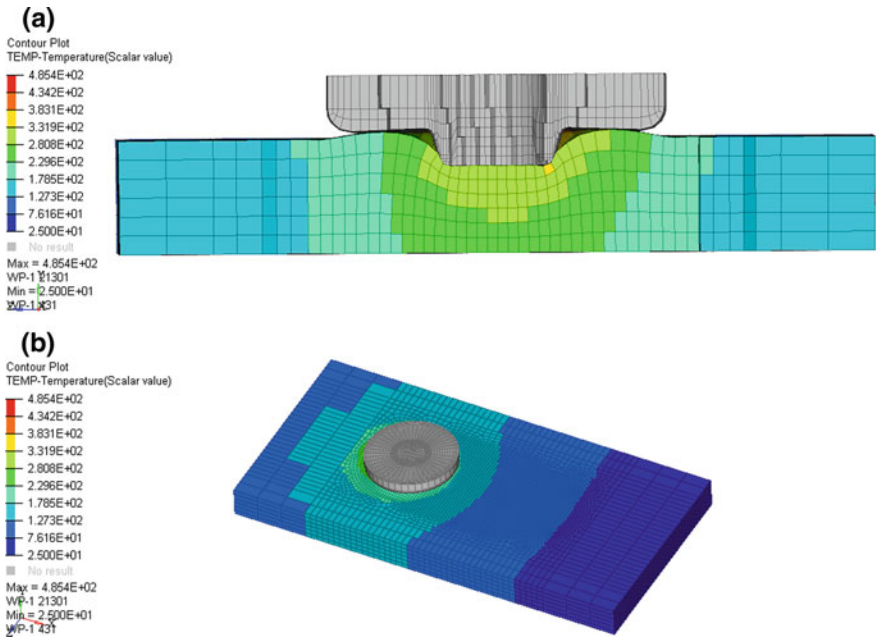


Fig. 5 The behaviour of the welding during the plunging step a cross section, b 3D view

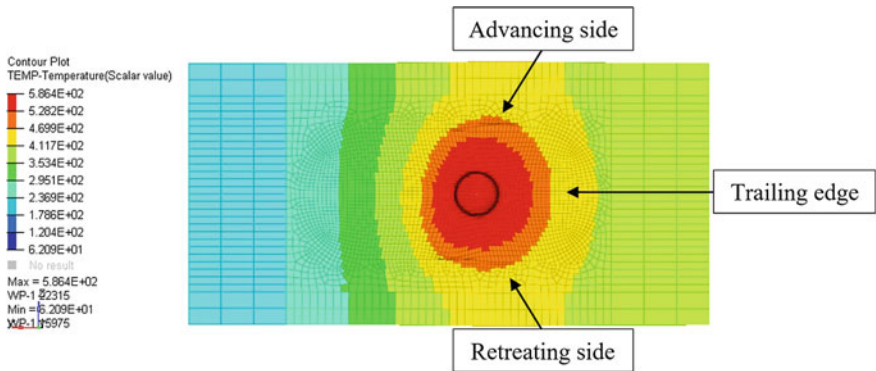


Fig. 6 Horizontal section of the welding

Figure 7 indicates that as the tool transfers across the vertical direction, the welding temperature increases. Besides, there is a “V” shape pattern for the temperature. The main reason for this pattern is due to the higher convection of the workpiece from the bottom surface. It needs to be noted that this matter affects the grain size of the thermo mechanical affected zone (TMAZ) and the heat affected zone (HAZ) [20]. In addition, an “onion ring” (bands of textures) structure is observed in the welding

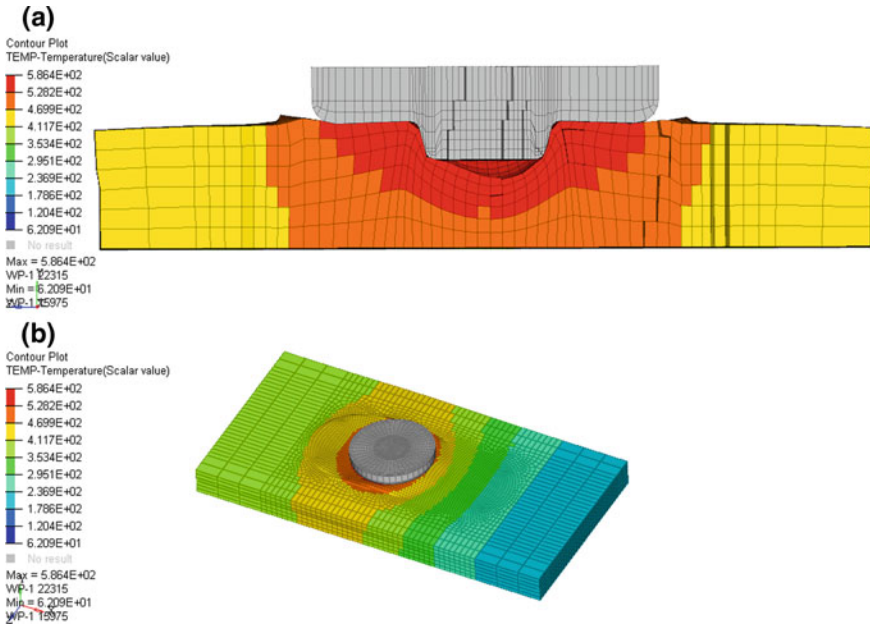


Fig. 7 Welding temperature distribution **a** cross section, **b** 3D view

area. The main reason of this kind of structure is the higher mixing of the material in the centre of the weld.

It is also observed that, temperature changes are highly influenced by the welding rotating speeds and the welding transverse movement. It was detected that, as the tool rotating speed is increased, the joint maximum temperature was also increased to 365 °C at the rotating velocity of 1600 RPM and the transverse velocity of 40 mm/min. Conversely, the welding temperature was decreased as the transverse speed increased [21–23]. Moreover, the differences of the temperature in the stirring zone were generally described as a quasi-steady behaviour, but as the distance from the welding centre line increases, the quasi-steady behaviour disappeared. Furthermore, the results showed that during all stages of the welding, the maximum temperature of the welding is less than the melting temperature of 6061-T6 aluminium alloy that is around 580 °C [24].

4 Conclusions

In this work finite element modelling of friction stir welding (FSW) is done in order to investigate the behavior of the heat. Altair® Software was used for modelling the process because of its powerful abilities in creating high quality mesh. From

the results it was investigated that, the heat produced by shoulder is higher (60 °C) and there is an asymmetrical pattern for the temperature and the temperature of the welding advancing side is higher around 30 °C. Moreover, at the constant transverse speed, when the rotational speed increased, temperature increased as well. Finally, the simulated model was validated with experiments and published papers and a good correlation between the results is achieved.

Acknowledgements The authors would like to acknowledge the financial support from Universiti Teknologi PETRONAS (UTP), Bandar Seri Iskandar, Perak Darul Ridzuan, Malaysia and the financial support from YUTP-FRG grant cost center 0153AA-H18. Moreover, the authors would like to thank Altair Engineering Sdn Bhd, Malaysia and professor Wallace Kaufman for their endless support and collaboration.

References

1. Su H, Wu CS, Bachmann M, Rethmeier M (2015) Numerical modeling for the effect of pin profiles on thermal and material flow characteristics in friction stir welding. *Mater Des* 77:114–125
2. Meyghani B, Awang MB, Emamian SS, Mohd Nor MKB, Pedapati SR (2017) A comparison of different finite element methods in the thermal analysis of friction stir welding (FSW). *Metals* 7:450
3. Meyghani B, Awang M, Emamian S, Khalid NM (2017) Developing a finite element model for thermal analysis of friction stir welding by calculating temperature dependent friction coefficient. In: 2nd international conference on mechanical, manufacturing and process plant engineering, pp 107–126
4. Miles M, Nelson T, Gunter C, Liu F, Fourment L, Mathis T (2018) Predicting recrystallized grain size in friction stir processed 304L stainless steel. *J Mater Sci Technol*
5. Argesi FB, Shamsipur A, Mirsalehi SE (2018) Dissimilar joining of pure copper to aluminum alloy via friction stir welding. *Acta Metall Sinica (English Letters)* 31:1183–1196
6. Khandkar M, Khan JA, Reynolds AP (2003) Prediction of temperature distribution and thermal history during friction stir welding: input torque based model. *Sci Technol Weld Joining* 8:165–174
7. Fehrenbacher A, Duffie NA, Ferrier NJ, Pfefferkorn FE, Zinn MR (2014) Effects of tool–workpiece interface temperature on weld quality and quality improvements through temperature control in friction stir welding. *Int J Adv Manuf Technol* 71:165–179
8. Dialami N, Chiumenti M, Cervera M, de Saracibar CA (2015) Challenges in thermo-mechanical analysis of friction stir welding processes. *Arch Comput Method Eng* 1–37
9. Dialami N, Chiumenti M, Cervera M, Segatori A, Osikowicz W (2017) Enhanced friction model for friction stir welding (FSW) analysis: simulation and experimental validation. *Int J Mech Sci* 133:555–567
10. Su H, Wu C, Pittner A, Rethmeier M (2014) Thermal energy generation and distribution in friction stir welding of aluminum alloys. *Energy* 77:720–731
11. Meyghani B, Awang M, Emamian S (2016) A comparative study of finite element analysis for friction stir welding application. *ARPN J Eng Appl Sci* 11:12984–12989
12. Ansari MA, Samanta A, Behnagh RA, Ding H (2018) An efficient coupled Eulerian-Lagrangian finite element model for friction stir processing. *Int J Adv Manuf Technol* 1–14
13. Meyghani B, Awang M, Emamian S, Nor MKBM (2018) Thermal modelling of friction stir welding (FSW) using calculated young's modulus values. In: *The advances in joining technology*. Springer, pp 1–13
14. Sun Z, Wu C, Kumar S (2018) Determination of heat generation by correlating the interfacial friction stress with temperature in friction stir welding. *J Manuf Process* 31:801–811

15. Jaffarullah MS, Nur' Amirah Busu CYL, Saedon J, Armansyah MSBS, Jaffar A (2015) Simulation analysis of peak temperature in weld zones during friction stir process. *J Teknol* 76:77–81
16. Meyghani B, Awang M, Emamian S, Akinlabi E (2018) A comparison between temperature dependent and constant Young's modulus values in investigating the effect of the process parameters on thermal behaviour during friction stir welding: Vergleich zwischen den temperaturabhängigen und konstanten Elastizitätsmodulwerten in der Untersuchung der Prozessparameter auf die Wärmewirkung beim Rührreißschweißen. *Materialwiss Werkstofftech* 49:427–434
17. Meyghani B, Awang M, Emamian S (2017) A mathematical formulation for calculating temperature dependent friction coefficient values: application in friction stir welding (FSW). *Defect Diff Forum* 379:73–82
18. Su H, Wu C, Pittner A, Rethmeier M (2013) Simultaneous measurement of tool torque, traverse force and axial force in friction stir welding. *J Manuf Process* 15:495–500
19. Mishra RS, De PS, Kumar N (2014) Fundamentals of the friction stir process. In: *Friction stir welding and processing*. Springer, pp 13–58
20. Abdul-Sattar M, Tolephih MH, Jweeg MJ (2012) Theoretical and experimental investigation of transient temperature distribution in friction stir welding of AA 7020-T53. *J Eng* 18:693–709
21. Emamian S, Awang M, Hussai P, Meyghani B, Zafar A (2016) Influences of tool pin profile on the friction stir welding of AA6061. *ARP J Eng Appl Sci* 11:12258–12261
22. Emamian S, Awang M, Yusof F, Hussain P, Mehrpouya M, Kakooei S et al (2017) A review of friction stir welding pin profile. In: Awang M (ed) 2nd international conference on mechanical, manufacturing and process plant engineering. Springer, Singapore, pp 1–18
23. Emamian S, Awang M, Yusof F, Hussain P, Meyghani B, Zafar A (2018) The effect of pin profiles and process parameters on temperature and tensile strength in friction stir welding of AL6061 alloy. In: *The advances in joining technology*. Springer, pp 15–37
24. Meyghani B, Awang MB (2018) Prediction of the temperature distribution during friction stir welding (Fsw) with a complex curved welding seam: application in the automotive industry. *MATEC Web Conference*, vol 225, p 01001